P1.30

IMAGER CAPABILITY ON CLOUD CLASSIFICATION USING MODIS

Zhenglong Li, Jun Li
Cooperative Institute for Meteorological Satellite Studies (CIMSS), University of Wisconsin-Madison
Paul Menzel, and Timothy J. Schmit
Office of Research and Applications, NOAA/NESDIS, Madison, Wisconsin

1 INTRODUCTION

Clouds play a very important role in earth-atmosphere system. Clouds significantly affect the heat budget by reflecting short-wave radiation (Hobbs and Deepak 1981) and absorbing long-wave radiation (Hunt 1982). Clouds also emit long-wave radiation. Those are the most fundamental optical characteristics of clouds. The real process is much more complicated. For example, one of the undetermined types of clouds is very thin cirrus that can act as clear sky (Liou 1986). Most solar radiation can pass through thin cirrus clouds with very little loss of energy. But cirrus clouds absorb long-wave radiation strongly, increasing the green house effect.

Accurate and automatic cloud detection and classification using satellite data is useful for many applications. It may help to better understand the global circulation. Most General Circulation Models (GCMs) use parameterization schemes to describe cloud-radiation process because the scale of cloud microphysics is much smaller than grid scale of these models. Better understanding of cloud classification will improve the retrieval of cloud top pressure, optical depth, effective radius (Frey et al. 1999; Li et al. 2001), all of which will benefit the parameterization schemes for GCMs (Yao and Del Genio 2002). Retrieval of profiles of atmospheric temperature, water vapor and ozone from GOES sounder measurements is based on good cloud detection (Hayden 1988). Clear, single and/or multilayer cloud information from MODIS measurements within a single AIRS footprint will greatly enhance the cloud clearing of partly cloudy AIRS radiances (Susskind et al.1998; Li et al. 2004).

We can divide cloud classification methods into two types. One is physically-based. These methods mainly use a set of thresholds (both static and dynamic) of albedo, brightness temperature (BT) and brightness temperature difference (BTD) (Ackerman et al. 1998). Spatial variance/ texture are also proved to be useful (Foody 1988). These methods can fail in the situation that there exist multilayered clouds or the cloud coverage is smaller than the instrument's field-of-view (FOV) size or clouds have variant emissivity. These methods were mainly developed during 1980s and early 1990s. After that time, with the improvement of computer speed, many researchers use mathematical or statistical methods to do cloud classification and detection. Methods, such as neural network (Key et al. 1990), Bayesian methods, clustering analysis or maximum likelihood (ML) (Li et al. 2002), fuzzy logic (Baum et al. 1997) have provided impressive results on cloud detection and classification. However, these methods may have some short-comings which prevent them from global usage. For example, neural network needs training sets which are region-based; Bayesian methods need information of the distribution of the data, which is now assumed to be normal distribution while the actual data might not be Gaussian. Obviously, prospective methods are those that succeed in combining the physically-based and mathematically-based methods.

Operational imagers on both polar orbiting and geostationary satellites are developed for monitoring the global evolution of the environment and clouds.

Corresponding author address: Zhenglong Li, SSEC/CIMSS, University of Wisconsin-Madison, 1225 West Dayton Street, Madison, WI 53706; e-mail: zhenglong.li@ssec.wisc.edu

For example, AVHRR/3 is a 6-band imager on the NOAA satellites and provides global cloud observations operationally, while the current GOES-12 imager provides hemispheric cloud observations in every 25 minutes. Future advanced imager VIIRS will replace AVHRR/3 on the NPOESS, while ABI will replace the current GOES imager on GOES-R and beyond for operational applications. One important question is how the advanced imagers (VIIRS and ABI) improve the current imagers (AVHRR/3 and the current GOES imager) in operational observation of clouds.

In order to simulate the capability of various imagers (current and advanced) on cloud detection and classification, MODIS data are used in the study. The ML algorithm is used for the surface and cloud type classification. This method highly depends on initialization. MODIS cloud mask product is used as initialization in the classification for all imagers. With the high quality of MODIS cloud mask data, the ML algorithm is used to compare different imagers to demonstrate their different capabilities on cloud detection and classification. MODIS classification is used as the standard for the evaluation of various imager sensors.

In the second section, data and different imagers are introduced. In third section, the ML algorithm is introduced. In the fourth section, the capability of MODIS on cloud classification is demonstrated and two cases are used to compare different imagers.

2 DATA

MODIS Data

Three types of data are used in the MODIS classification. Radiances are of the most import--they provide the primary information for surface and cloud types. In some situations, variance or texture images (Coakley and Bretherton 1982; Uddstrom and Gray 1996) and brightness temperature differences (BTD) also show their outstanding performance in detecting cloud and surface types (Liu 2004). Table 1 shows all the data used in MODIS classification. LSD means local standard deviation, also known as variance or texture images, and is given by

$$LSD(i,j)=\left[\sum_{m,n=-1}^{1}(x(i+m,j+n)-\bar{x})^2\right]^{1/2}$$

where $\bar{x}$ is the mean of 3 by 3 FOV area.

Table 1. Data used in MODIS and other sensors classification

Data	MODIS	ABI	AVHRR/3	GOES	MSG1	VIIRS
BAND1	Y	Y	Y	Y	Y	Y
LSD-1	Y	Y	Y	Y	Y	Y
BAND2	Y	Y	Y		Y	Y
LSD-2	Y	Y	Y		Y	Y
BAND3	Y	Y				
LSD-3	Y					
BAND4	Y					Y
LSD-4	Y					Y
BAND5	Y					Y
LSD-5	Y					Y
BAND6	Y	Y	Y		Y	Y
LSD-6	Y	Y	Y		Y	Y
BAND7	Y	Y				Y
LSD-7	Y	Y				Y
BAND17	Y					
BAND18	Y					
BAND19	Y					
BAND20	Y		Y			Y
BAND22	Y	Y		Y	Y	
BAND23	Y					Y
BAND24	Y					
BAND25	Y					
BAND26	Y	Y				Y
BAND27	Y	Y		Y	Y	
BAND28	Y	Y			Y	
BAND29	Y	Y			Y	Y
BAND31	Y	Y	Y	Y	Y	Y
LSD-31	Y	Y	Y	Y	Y	Y
BAND32	Y	Y	Y	Y	Y	Y
LSD-32	Y	Y	Y	Y	Y	Y
BAND33	Y	Y		Y	Y	
BAND34	Y					
BAND35	Y					
NDVI	Y	Y	Y		Y	Y
NDSI	Y					Y
BT11-12	Y	Y	Y	Y	Y	Y
BT8.6-11	Y	Y			Y	Y
BT11-6.7	Y	Y		Y	Y	
BT3.9-3.7	Y					
BT11-3.7	Y		Y			Y
BT12-4	Y					Y
BT13.7-14	Y					
BT11-3.9	Y	Y		Y	Y	
Number of Parameters	24	13	6	6	11	12

Other image Sensors

MODIS has 36 bands, much more than most other image sensors. Thus, MODIS data with the ML algorithm can be used to simulate other sensors to

compare their capabilities on cloud classification. For example, to simulate AVHRR/3 cloud classification using ML algorithm, we just use MODIS bands 1, 2, 6, 20, 31 and 32 as well as corresponding variance data and BTD data. For those bands that MODIS doesn't have (i.e. ABI band 6, 2.26 um), the nearest band is used as a substitution. Although spatial resolution has very important effects on classification, we will not include it in this study until the discussion section. Therefore, the resolution is 1 km for all imagers in the simulation, which is the same as MODIS.

ABI

The Advanced Baseline Imager (ABI) is the imager instrument onboard the future Geostationary Operational Environmental Satellites (GOES-R), which will be launched in 2012 (Gurka and Dittberner, 2001). The ABI expands the spatial resolution to 0.5 km for visible bands, 1.0 km for other visible/NIR bands, and 2km for IR bands (Schmit et al. 2004). Within 16 bands of ABI, 13 are selected for classification.

AVHRR/3

The Advanced Very High Resolution Radiometer (AVHRR/3) is a six bands imaging radiometer, onboard NOAA-K, L, M since 1998, with a resolution 1.1km. Compared with previous AVHRR, a new band 3A at 1.6 μm is designed to discriminate snow/ice.

The current GOES Imager

Currently, Geostationary Operational Environmental Satellite (GOES) have five satellites (GOES I-M). The GOES Imager has a five band multi-spectral capability on GOES I-L with a sixth band available on GOES-12 (Schmit et al. 2001). For maximum performance, all the six bands are used.

MSG-1

Meteosat Second Generation (MSG)—also called MET-8, a completely new series of European geostationary meteorological satellites, is a cooperation programme of ESA (European Space Agency) and EUMETSAT (European Organisation for the Exploitation of Meteorological Satellites). The main instrument on board is SEVIRI (Spinning Enhanced Visible and Infrared Imager), a 12-band radiometer providing images of the Earth disc with cloud and surface information (Schmetz et al. 2002). Among the 12 bands, 11 are suitable for classification.

VIIRS

The Visible Infrared Imaging Radiometer Suite (VIIRS), a 22-band multi-spectral scanning radiometer, a new generation of MODIS, will replace OLS and AVHRR/3 on board the NPOESS Preparatory Project (NPP) satellite in 2006, and will fly on National Polar Orbiting Environmental Satellite System (NPOESS) satellites in around 2010. The resolution for imagery is 375m, while for moderate is 750m. 12 bands are suitable for classification.

Table 1 shows the data used by each sensor for cloud classifications used in this study.

3 ML CLASSIFICATION ALGORITHM BASED ON THE MODIS CLOUD MASK

Classification or clustering of the radiances and local spatial distribution of the radiances is an important part of data analysis and image segmentation. A group or cluster refers to a class of data that has a similar appearance (i.e., for MODIS images, it can be a particular surface type or cloud cover). Basic data clustering does not need any external information for its completion.

In general, the distribution of each class presented in the MODIS image data can be approximated by a multivariate normal distribution, or locally normal distribution (Lee et al. 1999), and the classification procedure can be performed by the well-known ML or quadratic classifier (Haertel and Landgrebe 1999)

$$G_i(\mathbf{X}) = -(\mathbf{X} - \boldsymbol{\mu}_i)^{\mathrm{T}}\boldsymbol{\Sigma}_i^{-1}(\mathbf{X} - \mu_i) - \ln|\boldsymbol{\Sigma}_i| + 2\ln P(\omega_i), \quad (1)$$

with ω_i being a particular class, X an unlabeled vector of a pixel spanning the space of the radiance and spatial distribution of the radiance, μ_i the class mean vector in that space, Σ_i the class covariance matrix, $P(\omega_i)$ the corresponding a priori probability for class ω_i, and $G_i(X)$ the discriminate function associated with class ω_i; subscript i is the index for the ith class. For simplicity, assuming that the probability $P(\omega_i)$ for each class ω_i is equal, a distance is defined to assign each pixel to particular class ω_i:

$$D_i(\mathbf{X}) = (\mathbf{X} - \boldsymbol{\mu}_i)^T \boldsymbol{\Sigma}_i^{-1} (\mathbf{X} - \boldsymbol{\mu}_i) + \ln|\boldsymbol{\Sigma}_i|. \quad (2)$$

Mathematically, the pixel X is assigned to class ω_i if $D_i(X) \leq D_j(X)$ for all $\omega_j \neq \omega_i$. (3)

The clustering algorithm can be described by the following steps:

Classify the MODIS measurements using the MODIS cloud mask, and calculate the mean vector and covariance matrix of each class within the MODIS cloud mask.

Table 2 mean value for different classes at different bands

	water	t.low	o.snow	f.snow	low	high	middle	other
BAND1	2.14	4.9	6.89	16.85	18.38	31.72	23.2	14.14
LSD-1	0.46	2.58	1.87	2.17	1.93	0.79	1.08	2.08
BAND2	1.09	6.23	10.85	19.49	21.07	34.76	25.67	17.36
LSD-2	0.45	2.68	1.96	2.19	2.21	0.9	1.2	2.26
BAND3	6.46	8.94	10.16	19.18	21.4	34.08	25.79	17.27
LSD-3	0.39	2.11	1.53	1.8	1.52	0.71	0.9	1.65
BAND4	3.57	6.16	7.76	16.82	18.52	30.95	22.94	14.48
LSD-4	0.43	2.31	1.68	1.95	1.7	0.72	0.97	1.84
BAND5	0.51	4.35	7.78	11.17	15.53	27.27	18.93	11.99
LSD-5	0.3	1.53	1.16	1.2	1.73	0.87	0.95	1.44
BAND7	0.26	1.09	1.91	1.63	7.11	9.77	8.01	3.87
LSD-7	0.23	0.41	0.4	0.18	1.16	0.5	0.55	0.71
BAND17	0.88	5.5	9.71	16.65	18.27	31.14	22.3	14.81
BAND18	0.64	3.63	6.43	10.22	11.39	23.36	14.65	8.66
BAND19	0.71	4.37	7.78	12.75	14.12	26.32	17.61	11.07
BAND20	273.06	267.34	264.31	259.02	276.84	266.19	272.24	269.65
BAND22	271.97	265.56	261.98	257.2	267.56	252.41	263.09	264.41
BAND23	269.42	263.12	259.58	256.08	261.45	247.4	257.73	260.19
BAND24	233.49	231.88	231.22	229.56	230.62	226.9	228.8	230.13
BAND25	249.86	245.92	243.89	241.1	242.12	230.08	239.55	242.47
BAND26	0.13	0.28	0.4	0.44	0.87	10.02	2.93	0.33
BAND27	242.14	240.23	239.88	238.32	238.24	225.29	233.06	238.5
BAND28	253.96	250.81	249.34	247.39	247.72	230.07	242.25	247.94
BAND29	270.81	263.71	259.62	256.04	256.45	234.93	249.47	258.62
BAND31	272.11	264.48	260	256.19	257.05	233.39	249.15	259.26
LSD-31	0.28	0.65	0.31	0.36	0.68	1.1	0.72	0.41
BAND32	271.49	264.17	260.03	256.05	256.71	232.66	248.6	259.13
LSD-32	0.34	0.72	0.36	0.4	0.72	1.12	0.75	0.48
BAND33	254.86	250.83	248.83	246.3	245.91	228.42	241.53	247.4
BAND34	244.08	241.51	240.38	239.09	238.06	225.37	234.79	238.81
BAND35	236.95	235.08	234.29	233.2	232.51	223.23	229.39	232.77
NDVI	-53.09	-6.14	32.79	12.99	10.99	7.48	8.31	15.58
NDSI	132.98	113.52	92.64	122.28	72.7	78.28	76.95	93.47
BT11-12	0.63	0.31	-0.03	0.13	0.36	0.74	0.55	0.13
BT8.6-11	-1.3	-0.77	-0.37	-0.16	-0.59	1.54	0.19	-0.65
BT11-6.7	29.97	24.25	20.12	18.39	18.36	8.06	15.67	20.78
BT3.9-3.7	-1.09	-1.78	-2.33	-2.11	-9.31	-13.77	-9.84	-5.26
BT11-3.7	-0.95	-2.86	-4.32	-3.8	-20.05	-32.8	-22.93	-10.37
BT12-4	2.07	1.06	0.45	-0.16	-4.91	-14.75	-8.34	-1.05
BT13.7-14	7.12	6.43	6.09	5.87	5.61	2.06	4.64	5.89
BT11-3.9	0.15	-1.08	-1.99	-1.69	-10.73	-19.03	-13.1	-5.1

Calculate the distances between the vector of each pixel and mean vectors of different classes, and assign the pixel to the nearest class.

Update the mean vector and covariance matrix of each class after all pixels have been reassigned to the nearest classes.

Repeat steps 2 and 3 until convergence criteria are met. In this paper, if the sum of the off-diagonal elements for each class in the classification matrix is less than 6%, the iterations end. In general, approximately 6 to 7 iterations are needed for a final ML classification result.

4 CASE STUDY

Case 1: High latitude case: 18:55 Feb 4, 2004

Interpret MODIS classification

Cloud classification in high latitude areas during the winter is always challenging because of the high reflectance of surface that is often covered by snow (Allen et al. 1990). In this case, we will demonstrate the capability of MODIS classification and compare with other sensors. As mentioned, MODIS cloud mask is used to initialize the ML algorithm.

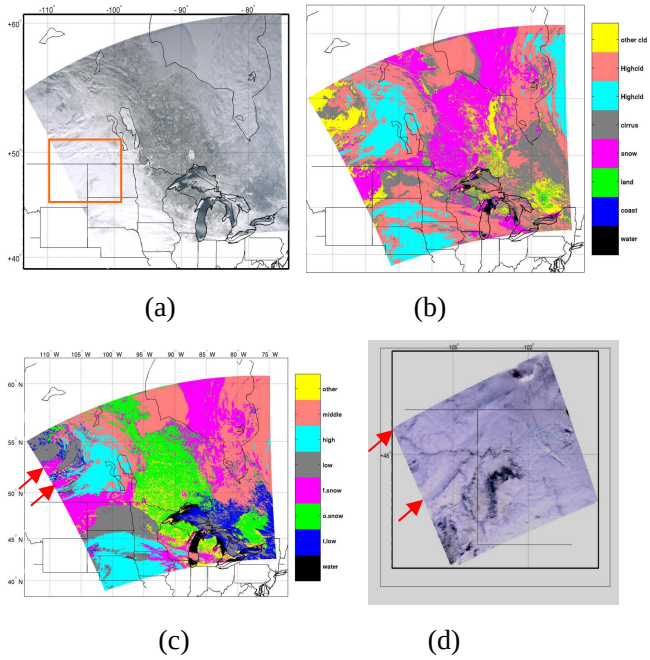

Fig 1 (a) True color image, (b) MODIS cloud mask (c) MODIS cloud classification for case 18:55 Feb. 4, 2004. (d) zoom of the red rectangle in (a). Notice the two rivers which are labeled by two arrows. (d) is contrast-stretched to better shown the features.

Fig 1 (a)-(c) are true color image (based on MODIS band 1, 2 and 4), MODIS cloud mask and MODIS classification separately. Basically, classification has the same pattern as cloud mask. To

identify each class in the classification results, true color image as well as other information is used.

There are 5 types of clouds in the classification. The high clouds/ice clouds class is verified because it has very low BT (233.39 K) in band 31 (see table 2 for mean value for each class at different bands). Low clouds have relatively high reflectance in VIS/NIR bands and high BT in band 31. Also BT_{11}-BT_{12} has a greater value than $BT_{8.6}$-BT_{11}, which indicates low clouds. Middle/mixed clouds have spectral characteristics between high clouds and low clouds--brighter and colder than low clouds, and darker and warmer than high clouds; variance of VIS/NIR bands larger than high clouds and less than low clouds; variance of BT31 larger than low clouds and less than high clouds. The fourth class of clouds is thin low clouds ("t.low" in table 2). It is thin clouds because of very low reflectance of VIS/NIR bands, very high BT in band 31 and it is verified by the fact that a large part of this class is over Lake Superior, which indicates that it is not snow. Also it doesn't show the characteristics of ice clouds. Other classes are mixed surface type, or other clouds. Some of them are clouds (areas between Lake Michigan and Lake Huron), some of them are ice (west of Lake Superior), and some of them are snow (Green Bay). However, these classes contain only small percentage of pixels.

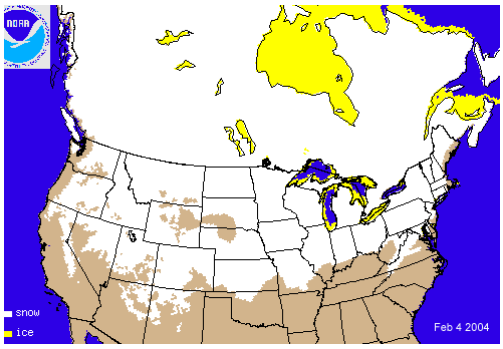

Fig 2 Snow and ice map from NOAA.

For clear areas, there are three classes in this case. The class of water is the easiest to verify, as can be seen from true color image. It corresponds to clear open water. Fresh snow ("f.snow" in table 2) is a little hard to verify from the true color image, especially for the areas in Montana and North Dakota. However, some tiny details ensure that snow covers this area. Actually, at least two rivers (Missouri and Yellowstone) can be recognized in this true color image if zooming in that part (arrowed in Fig 1 (d)), which indicates it is clear sky. It's fresh snow because it has larger

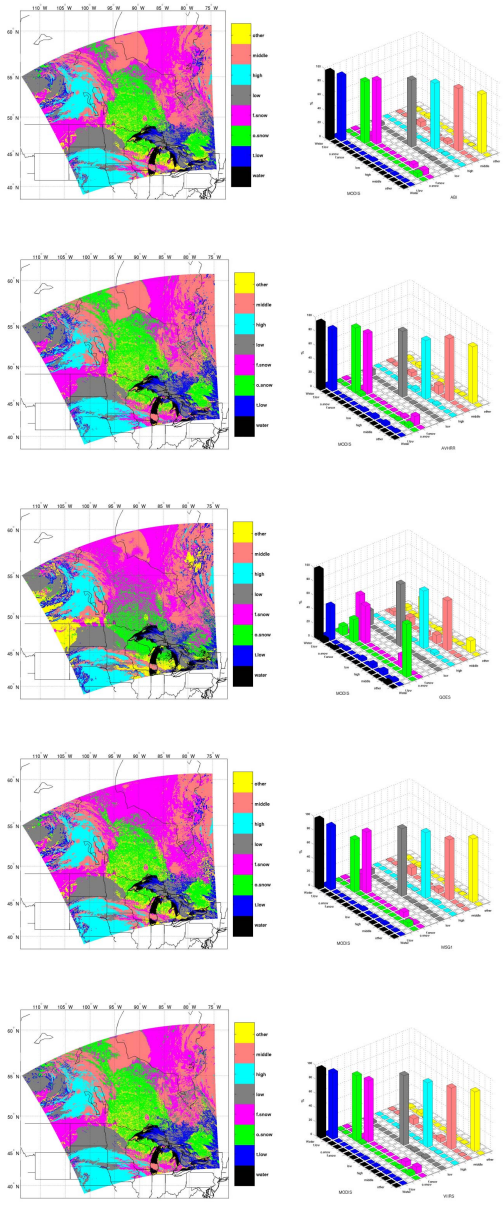

Fig 3 Classification by different sensors (left column) and corresponding classification matrix (right column) for case 18:55 Feb. 4, 2004
From top to bottom: ABI, AVHRR/3, GOES, MSG1, VIIRS

reflectance than the other. Fig 2 is snow and ice cover map from the National Oceanic and Atmospheric

Administration (NOAA; see http://www.nohrsc.nws.gov/index.html). Over Hudson Bay, the temperature was so low that the whole bay is frozen. Obviously, it is covered by snow over ice. The green area is also classified as snow. Both pink and green are snow, but they are different: pink denote fresh snow while green is old snow ("o.snow" in table 2)------the pink has a higher reflectance than green, and a slighted lower surface temperature (BT_{11}), with a difference less than 4 degree. This difference is mainly caused by the different reflectance of solar radiation, which results in different absorption of solar radiation.

Although the MODIS cloud mask has the same pattern as the classification, we can still see the improvement by the ML classification algorithm. For example, classification discriminates fresh snow from old snow, especially two misclassified areas which locate on (110 °W, 52.5°N) and (108°W, 51°N). These two areas are labeled by red arrows in (c). Also classification of clouds has some improvement.

However, there is one type of cloud that is not detected: thin cirrus. In this case, there are some thin cirrus over Lake Michigan. But it is too thin to be classified.

Another way to verify the MODIS classification is to compare results with GOES animation (see http://angler.larc.nasa.gov/armsgp/). Both visible and IR bands can show the movement of clouds and stability of clear surface that is covered with snow.

Classification by different sensors

Fig 3 shows the results of classification by different image sensors. For each sensor, there are two figures to interpret the results. The left is the classification result, while the right is the classification matrix C(i , j) between the results by this sensor and MODIS, which indicates the percentages of pixels of the i^{th} class of MODIS classification assigned to j^{th} class of the current classification. For example, C(14,4)=6.51% means 6.51% of other cloud in MODIS classification is changed to class of land in ABI classification. Thus, larger value of diagonal elements indicates better results (more similar to the MODIS classification). Obviously, the percentage for each class in MODIS classification is 100%, or

$$\sum_{i=1}^{15} C(i, j) = 100\% .$$

Generally, all the sensors produce about the same pattern of classification except the current GOES imager, which misclassifies some of middle cloud as clear. This is because there is only one visible band in the current GOES imager. The current GOES imager also has problems detecting thin/low clouds and old snow. However, for each class, there are some differences among the sensors.

Table 3 classification matrix for different sensors 18:55 Feb 4, 2004 (case 1)

	water	t.low	o.snow	f.snow	low	high	middle	Other	SL
ABI	97.41	93.72	88.60	91.7.0	96.34	94.77	90.16	84.63	92.17
AVHRR/3	94.79	87.09	92.40	85.92	93.26	83.21	88.62	80.00	88.16
GOES	98.50	49.00	32.89	53.35	88.58	81.92	70.94	16.75	61.49
MSG1	97.43	90.01	74.39	86.29	95.51	92.74	85.45	89.85	88.96
VIIRS	96.72	93.89	92.59	87.16	98.47	91.28	86.62	84.26	91.37
mean	96.97	82.74	76.17	80.88	94.43	88.78	84.36	71.10	

Table 3 is the diagonal elements C(i, i) of classification matrix for each sensor. For example, the percentage of low clouds for the current GOES imager is 88.58%, which means 88.58% of low clouds in MODIS classification is retained in the current GOES imager classification. Obviously, the larger diagonal percentage, the better classification for the sensor. We define significance of likelihood as mean of diagonal elements of the matrix, SL=E(C(i,i)). Obviously, this value can be used to compare the capability of different sensors. The "mean" in the table is the mean value of all columns, which is useful to compare the easiness to discriminate different classes.

As expected, the class of water has the highest mean percentage, which means all the sensors have the capability to detect open water. This is reasonable since open water is very homogeneous for almost all the bands. Low clouds are the second easiest to detect. They have a mean percentage as high as 94.43%, which indicates the classification of low clouds has a high reliability for all the five sensors. High clouds also have a good reliability. ABI, MSG1

and VIIRS have the percentage above 91.28%. Although AVHRR/3 and GOES have relatively low percentage (just more than 80%), the pattern is almost the same, as can be seen from Fig 3. The main difference comes from the edge between high clouds and middle clouds. The reason that middle level clouds have smaller percentages than high and low level clouds is that middle level clouds usually have mixed phase, while high and low clouds usually have only one phase. For snow and thin low clouds, not all the sensors have acceptable results. ABI, MSG1 and VIIRS always have percentage above mean, while GOES has a percentage far below average. The results of AVHRR/3 will be discussed later.

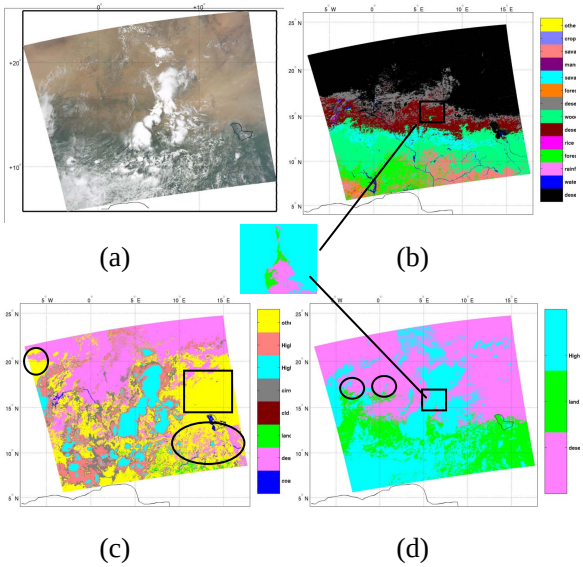

Fig 4 (a) True color image, (b) surface mask, (c) MODIS cloud mask (d) MODIS cloud classification for case 13:00 Aug 22, 2004.

From Figure 3 and Table 3, it is clear that the more spectral bands, the better results. ABI has 13 spectral parameters used in the classification and it has the mean percentage of 92.17, the maximum of all; VIIRS has 12 spectral bands in the classification and has the second maximum mean. The current GOES imager has only 6 spectral bands, and it has the minimum mean percentage. However, this is only for the general situation. If the comparison is based on a specific class, this might not be always true. For the best three sensors: ABI, MSG1, VIIRS, all of them have some maximum percentages. For example, ABI has the maximum of fresh snow, high clouds, middle clouds; MSG1 has the maximum of other clouds; VIIRS has some maximum of thin low clouds, old snow, low clouds. Obviously, for a certain class/day, we can't say the more bands, the better results.

Case 2: desert case, 13:00 Aug 22, 2004

Because desert has very large reflectivity, it is often misclassified as low cloud. In this case, we will focus on correctly identifying the desert. Fig 4 (a)-(c) are true color, surface mask, MODIS cloud mask and MODIS cloud classification respectively. The former two will be used as reference to interpret MODIS classification. The image of surface mask is also at 1km resolution. It provides the information about the coverage. Since our interest is to identify the desert, only three classes (desert, land and clouds) are examined. In this way, the capability of discriminating desert from land is examined as well as discriminating cloud from clear (both land and desert).

Table 4 classification matrix for different sensors 13:00 Aug 22, 2004 (case 2)

	desert	land	cloud	SL
ABI	95.97	88.09	98.51	94.19
AVHRR/3	95.05	83.39	96.88	91.77
FY1C	95.05	83.39	96.88	91.77
GOES	92.86	23.26	87.29	67.80
MSG1	97.00	79.44	95.15	90.53
VIIRS	97.71	88.79	98.65	95.05
mean	95.72	72.59	95.30	

From the true color image, most of the desert area is clear. Those covered by clouds are detected successfully in the cloud mask image. However, many of the clear desert areas, which can be verified by the true color image, are misclassified as other clouds in cloud mask image. For example, in the east-south part of Mauritania (black-circled in fig 4 (c)), it is mostly clear desert, which is classified as other clouds in cloud mask. Also, the east part of Niger is clear desert (black rectangle), which can be verified by true color image too, and it is also classified as other clouds. Another large misclassification is that cloud mask misclassifies clear land as desert (black ellipse). Between 10°N and 15°N, most of the clear areas are classified as desert. However, from the surface mask image, we can see these areas are mainly covered by savanna and woods, especially the northwest of Burkina Faso and southwest of Chad, both of which

as covered by woods and savanna.

In the MODIS cloud classification mask, most of the clear desert is successfully classified. The line of 13°N is approximately a border between desert and land. North of it are mostly desert, including bare desert, semi desert shrubs and hot and mild grasses and shrubs; while south of it are mostly land, including tropical rainforest, tropical degraded forest, rice paddy and field, savanna and woody savanna etc. Here we treat areas of hot and mild grasses and shrubs as semi-desert. The MODIS classification can even

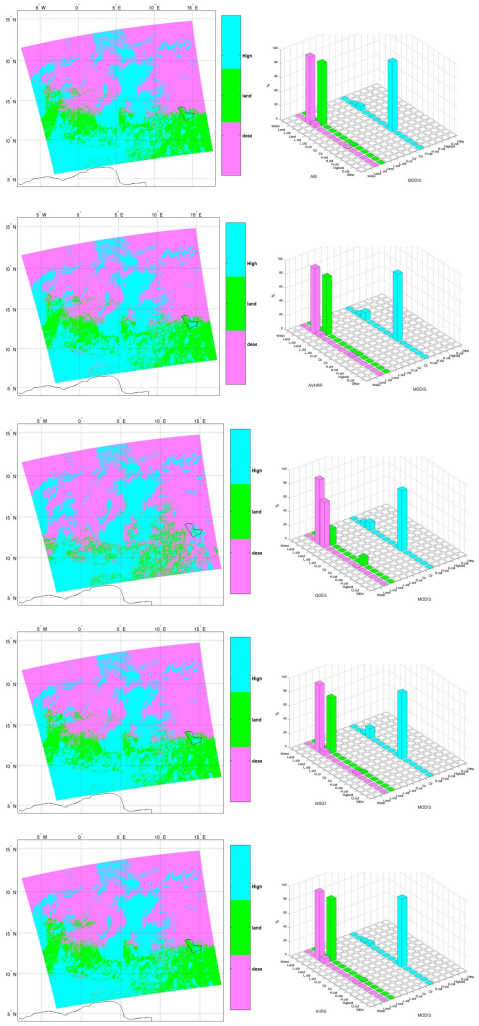

Fig 5 Classification by different sensors (left column) and corresponding classification matrix (right column) for case 13:00 Aug 22, 2004

From top to bottom: ABI, AVHRR/3, GOES, MSG1, VIIRS

detect small green areas surrounded by desert. In the surface mask image, there is a small area of woods located on 7°E and 15°N. In the MODIS cloud classification mask, we can recognize this wood area near the clouds (see the zoomed part). The south of the wood area is classified as desert, which is consistent with surface mask.

At the border between land and desert, there are some differences between the MODIS cloud classification mask and the surface mask. This is because the coverage of this area has strong seasonal variation. During rain season, this area is partly covered by green vegetations. The rain season of Mali and Niger is from June to September. As a result, more land is detected in the classification mask than the surface mask. Specifically, there are two relatively large areas located to the north of 15°N, which is circled in (d).

Most of the clouds over desert are detected very well in the MODIS classification mask comparing with the true color image. Notice the cumulus in the north is successfully classified as well. However, over the land, the detection is not very good, especially for very thin cloud. As we can see from true color image, most land areas are covered by clouds, especially the thin clouds. While in the MODIS classification mask, more than half of this area is classified as clear. In fact, detection of very thin clouds, both low clouds and high clouds, is still a challenge to this algorithm. However, here in this case, we mainly focus on the capability of discrimination of desert from low clouds.

Classifications by other sensors are shown in Figure 5 and table 4. Again, the MODIS classification mask is used as the standard.

All of the five sensors have very high percentage of desert comparing with MODIS, with the maximum 97.91 for VIIRS and minimum 92.86 for the current GOES imager. Unlike the cloud mask, this algorithm seldom misclassifies desert as cloud. Also, most of them detect clouds very well, with the maximum 98.65 for VIIRS. However, the current GOES imager is an exception. In the current GOES imager classification mask, many areas of clear land are classified as desert, which is obviously wrong, comparing with the true color image and surface mask image. Actually, this is the reason why the percentage of land from the current GOES imager is so small-----large amount of

land is classified as desert. Basically, except for the current GOES imager, other four sensors all have good capability to detect desert, clouds and land. As previous mentioned, the ABI and VIIRS have the best results since they have more bands than others. MSG1 has the third best results. Examining the difference among the MODIS, ABI, MSG1 and VIIRS classification results, it is found that the difference mainly comes from the border where different classes are adjacent. This is reasonable because in reality you can't find such an exact border (edge) to discriminate the desert from other land, and the clouds from clear land.

Although AVHRR/3 has the same number of bands as the current GOES imager, it gives better results. This can be partly explained by the difference between the two sensors. The main difference between AVHRR/3 and the current GOES imager is that the former has MODIS band 2 and 6, while the latter has MODIS band 33. This is the actual reason for the difference between the two classification results. MODIS band 33, the CO_2 spectral band (13.3 μm), has been widely used for cloud detection. This is the reason why the detection of clouds by the current GOES imager is acceptable (the percentage of clouds is 87.29% with 6.57% of desert and 11.25% of land from MODIS classification misclassified as clouds). Band 2 (0.86 μm) and 6 (1.64 μm) have been widely used for surface classification, snow, clouds etc. For AVHRR/3, we will discuss more in the next section.

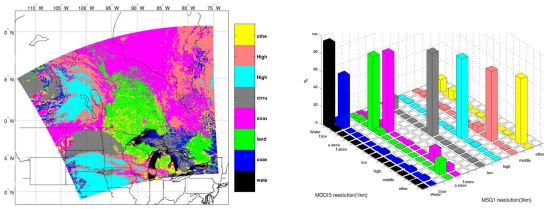

Fig 6 Classification by MSG1 at MSG1 resolution (left) and corresponding classification matrix (right) for case 1. The classification matrix is compared to MSG1 classification at MODIS resolution

5 DISCUSSIONS

In reality, there are mainly two reasons to constraint the performance of the different sensors. One is that the spatial resolution is not as high as MODIS, especially for AVHRR/3, GOES and MSG1. When the resolution is coarser, some information about spatial variant is also smoothed out. Figure 6 is the classification mask from MSG1 at the MSG1 spectral resolution (3 km). From the image and classification matrix, it is obvious that the spatial resolution plays a relatively important role in cloud classification. As the resolution reduces to 3 km, classes of thin low clouds, old snow, fresh snow, middle clouds are changed more than 10%. As for VIIRS, since it has a higher resolution than MODIS, better results are expected than what we have shown here.

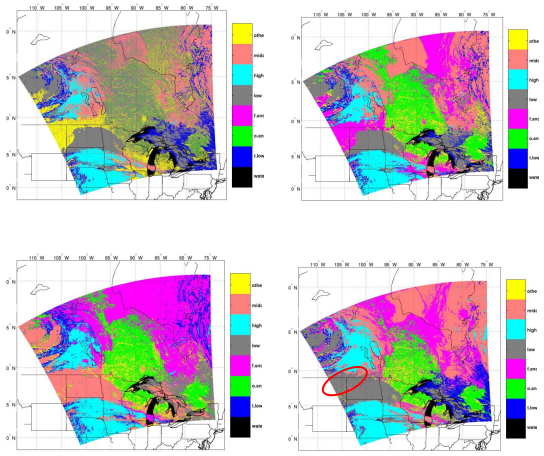

Fig 7 Classification by (a) noise-added AVHRR/3; (b) AVHRR/3 without band 6; (c) AVHRR/3 without band 20; (d) ABI without 3.7/3.9um

The other reason is that the measurement by MODIS has higher precision than most of the other sensors. Although AVHRR/3 has a similar resolution (1.1 km) as MODIS (1 km), the signal-to-noise ratio (SNR) is smaller than MODIS, which means the measured radiances by MODIS have less noise than by AVHRR/3. Figure 7(a) is the noise-added classification by AVHRR/3. Noise here is normally distributed with mean 0 and standard deviation 1/9, 1/9, 1/20, 0.12, 0.12, 0.12 K for AVHRR/3 6 bands. This is one reason that the AVHRR/3 can not give such good results as in our study. Also, in practice, band 3A (band 6 of MODIS, 1.64 μm) and 3B (band 20 of MODIS, 3.7 μm) are not available

simultaneously. Figure 7 (b) is the classification without band 6, while Figure 7(c) is the classification without band 20. As expected, the capability of AVHRR/3 is not as good as demonstrated in the two cases. Actually, the mean value of classification matrix is 66.21%, 91.88% and 57.44% respectively.

From Figure 7(b) and 7(c), it is found that band 20/22 (3.7/3.9 μm) is more important for cloud classification than band 6. For comparison, we calculate case 1 without 3.7/3.9 μm for ABI. Figure 7(d) is the results. Compared with regular ABI classification in Figure 3, the most evident difference is that the snow-covered clear surface in north of Montana and North Dakota (circled) is mis-classified as low clouds. The SL here is 80.47%. This means turning off band of 3.7um results in decreasing of SL as large as 20% for ABI. And in the AVHRR/3 case, the decreasing is 1-57.44%=43.56%.

6 CONCLUSIONS

An ML classification algorithm, which uses MODIS cloud mask as the initial condition, was used to compare the capability of different sensors to detect and classify surface/cloud types. The MODIS VIS/NIR/IR 1km resolution spectral information and some of the spatial information (variance) as well as radiance differences are used in the classification. Generally, the more spectral bands, the better results (much closer to the MODIS classification). Both ABI (13 parameters) and VIIRS (12 parameters) have the excellent classification results compared to MODIS. MSG1 has better classification than AVHRR/3. While AVHRR/3 has acceptable results, the current GOES imager classification is not as good as other imager sensors. Besides the number of bands, some specific bands are found very important for classification. It's because there is no MODIS bands 2 and 6 on the current GOES imager that its classification is much worse than the AVHRR/3. Also, for some specific classes, one can't tell ABI has better results than AVHRR/3 on cloud classification. This may be confusing because ABI has all AVHRR/3 bands (3.7 are almost same as 3.9). This is very useful information that may help improve the algorithm in the future.

7 ACKNOWLEDGEMENTS

This program is supported by NOAA ABI/HES program NA07EC0676 at CIMSS. The views, opinions, and findings contained in this report are those of the author(s) and should not be constructed as an official National Oceanic and Atmospheric Administration or U.S. Government position, policy, or decision.

8 REGERENCES

Allen, R. C., Jr., P. A. Durkee, and C. H. Wash, 1990: Snow/cloud discrimination with multispectral satellite measurements. *J. Appl. Meteor.,* **29,** 994–1004.

Baum, Bryan A., Vasanth Tovinkere, Jay Titlow, Ronald M. Welch, 1997: Automated Cloud Classification of Global AVHRR/3 Data Using a Fuzzy Logic Approach. *J. Appl. Meteor.* **36**, 1519-1540.

Coakley, Jr, J. A., and Bretherton, F. P., 1982, Cloud cover from high resolution scanner data: Detecting and allowing for partially filled fields of view. *Journal of Geophysical Research*, **87**, 4917–4932.

Foody, G. M., 1988, The effects of viewing geometry on image classification. *International Journal of Remote Sensing*, **9**, 1909–1915.

Frey, R. A., B. A. Baum,W. P. Menzel, S. A. Ackerman, C. C. Moeller, and J. D. Spinhirne, 1999: A comparison of cloud top heights computed from airborne lidar and MAS radiance data using CO2 slicing. *J. Geophys. Res.,* **104,** 24, 547–24 555.

Gurka J. J., and G. J. Dittberner, 2001: The next generation GOES instruments: status and potential impact. Preprint Volume. 5th Symposium on Integrated Observing Systems. 14-18 January, Albuquerque, NM., Amer. Meteor. Soc., Boston.

Haertel, V., and D. A. Landgrebe, 1999: On the classification of classes with nearly equal spectral response in remote sensing hyperspectral image data.

*IEEE Trans. Geosci. Remote Sens.,***37**, 2374–2385.

Hayden, C. M., 1988: GOES VAS simultaneous temperature moisture retrieval algorithm, *J. Appl. Meteor.*, **27**, 705-733

Hobbs, P. V. and Deepak, A. (editors), 1981, Clouds: T heir Formation, Optical Properties and Effects (New York: Academic Press), figure 2, p. 285.

Hunt, G. E., 1982, On the sensitivity of a general circulation model climatology to changes in cloud structure and radiative properties. Tellus, **34**, 29–38.
Key, J, J. A. Maslanik, and A. J. Schweiger, 1989: Classification of merged AVHRR/3 and SMMR Arctic data with neural networks. *Photogramm. Eng. Remote Sens.,* **55,** 1331–1338.

Lee, J. S., M. R. Grunes, T. L. Ainsworth, L. J. Du, D. L. Schuler, and S. R. Cloude, 1999: Unsupervised classification using olarimetric decomposition and the complex Wishart classifier. *IEEE Trans. Geosci. Remote Sens.,* **37**, 2249–2258.

Li, J, W. P. Menzel and A. J. Schreiner, 2001: Variational retrieval of cloud parameters from GOES sounder longwave cloudy radiance measurements. *J. Appl. Meteor.,* **40,** 312–330.

Li, J., W. P. Menzel, Z. Yang, R. A. Frey, and S. A. Ackerman, 2003: High-spatial-resolution surface and cloud-type classification from MODIS multi-spectral band measurements, *J. Appl. Meteorol.,* **42**, 204 - 226.

Li, J., W. P. Menzel, F. Sun, T. J. Schmit, and J. Gurka, 2004: AIRS subpixel cloud characterization using MODIS cloud products. *J. Appl. Meteorol.,* 43, 1083 - 1094.

Liou, KN, 1986: Influence of cirrus clouds on weather and climate processes: a global perspective. *Mon Wea Rev*, **114**, 1167–99.

Liu, Yinghui, Jeffrey R. Key, Richard A. Frey, Steven A. Ackerman and W. Paul Menzel, 2004: Nighttime polar cloud detection with MODIS, *Remote Sensing of Environment*, **92**, 181-194.

Schmetz, Johannes, Paolo Pili, Stephen Tjemkes, Dieter Just, Jochen Kerkmann, Sergio Rota, and Alain Ratier, 2002: An Introduction to Meteosat Second Generation (MSG). *Bull. Am. Meteorol. Soc.*, **83**, 977-992

Schmit, T. J., J. Li, M. M Gunshor, C. C Schmidt, W. P. Menzel, J. J. Gurka, and J. M. Sieglaff, 2004: Study Of The Advanced Baseline Imager (ABI) On The GOES-R And Beyond, *AMS IIPS meeting*. Seattle, WA

Schmit, T. J., E. M. Prins, A. J. Schreiner, and J. J. Gurka, 2001: Introducing the GOES-M Imager. *Natl. Wea. Dig.* **25**, 28-37.

Susskind, J., C. D. Barnet, and J. Blaisdell, 1998: Determination of atmospheric and surface parameters from simulated AIRS/AMSU sounding data: Retrieval methodology and cloud clearing methodology. *Adv. Space Res.,* **21**, 369–384.

Uddstrom,M. J., Gray, W. R., Murphy, R., Oien, N. A., and Murray, T., 1999, A Bayesian cloud mask for sea surface temperature retrieval. *Journal of Atmospheric and Oceanic Technology*, **16**, 117–132.

Yao, M and Del Genio, AD, 2002, Effects of Cloud Parameterization on the Simulation of Climate Changes in the GISS GCM. *J. Clim.* **15**, 2491-2504